Phase Distribution Phenomena for Simulated Microgravity Conditions: Experimental Work

Maneesh Singhal, Fabian J. Bonetto, and R.T. Lahey, Jr.
Rensselaer Polytechnic Institute
Troy, New York

March 1996

National Aeronautics and
Space Administration

FINAL TOPICAL REPORT

Phase Distribution Phenomena for Simulated Microgravity Conditions: Experimental Work

Maneesh Singhal, Fabian J. Bonetto, R.T. Lahey Jr.
Center For Multiphase Flow
Rensselaer Polytechnic Institute
Troy, NY 12180

1.0 INTRODUCTION

This report summarizes the work accomplished at Rensselaer to study phase distribution phenomenon under simulated microgravity conditions. Our group at Rensselaer has been able to develop sophisticated analytical models to predict phase distribution in two-phase flows under variety of conditions. These models are based on physics and data obtained from carefully controlled experiments that are being conducted here. These experiments also serve to verify the models developed.

2.0 ANALYSIS

2.1 Conservation Equations

The generic conservation equation for each phase is given by:

$$\frac{\partial}{\partial t}\rho\Psi + \nabla \cdot \rho\Psi\mathbf{v} = \nabla \cdot \mathbf{J} + \rho\mathbf{f} \tag{1}$$

The corresponding jump condition between components k and l is:

$$[\,(\rho\Psi(\mathbf{v}-\mathbf{v}_i) + \mathbf{J}) \cdot \mathbf{n}\,]_{kl} = M_i \tag{2}$$

where:

Ψ ...conserved quantity

$\mathbf{J}$ ...conserved quantity's flux

$\mathbf{f}$ ...conserved quantity's source density

M_i ...conserved quantity's interfacial source

Typical state variables are given in Table 1.

Table 1: State variables in generic conservation equations and jump conditions

Balance Principle	Ψ	J	f	M_i
Mass	1	0	0	0
Momentum	$\mathbf{v}$	$\mathbf{T}$	$\mathbf{g}$	m_i^s
Energy	$u + \frac{1}{2}v^2$	$\mathbf{T} \cdot \mathbf{v} - \mathbf{q}''$	$\mathbf{g} \cdot \mathbf{v} + r$	e_i^s
Enthalpy	h	$-\mathbf{q}''$	$r + \frac{1}{\rho}\left(\frac{dp}{dt} + \tau : \nabla \mathbf{v}\right)$	h_i^s

To obtain the conservation equations which govern the motion of turbulent dispersed solid/fluid flows, the generic equation is first multiplied by the phase indicator function, X_k, defined as:

$$X_k = \begin{cases} 1, & \text{if } x \in k \\ 0, & \text{otherwise} \end{cases}$$

, and then averaged over all the possible realizations (ensembles). Drew et. al. [1995] define ensemble averaging of a function F at position x and time t, for some particular realization μ, as:

$$F(\mathbf{x}, t) = \int_\varepsilon F(x, t; \mu) \, dm(\mu)$$

, where ε, ensemble, is the set of all the possible realizations. Also, if we consider a point on the interface while moving with it, we see that the phase indicator function, X_k, is a constant jump discontinuity. Therefore, its material derivative must be zero. That is,

$$\frac{D_i X_k}{Dt} = \frac{\partial X_k}{\partial t} + \mathbf{v}_i \cdot \nabla X_k \equiv 0. \tag{3}$$

By using the above equation and procedure, ensemble-averaged conservation equations for adia-

batic two-phase flow are obtained:

Mass Conservation

$$\frac{\partial \alpha_k \bar{\rho}_k}{\partial t} + \nabla \bullet \alpha_k \bar{\rho}_k \bar{\mathbf{v}}_k = \overline{\rho (\mathbf{v} - \mathbf{v}_i) \cdot \nabla X_k} \tag{4}$$

Momentum Conservation

$$\frac{\partial \alpha_k \bar{\rho}_k \bar{\mathbf{v}}_k}{\partial t} + \nabla \cdot \alpha_k \bar{\rho}_k \bar{\mathbf{v}}_k \bar{\mathbf{v}}_k = \nabla \cdot \overline{X_k \mathbf{T}_k} + \nabla \cdot \alpha_k \tau_k^{Re} + \alpha_k \bar{\rho}_k \bar{\mathbf{g}}_k + \overline{\rho (\mathbf{v} - \mathbf{v}_i) \cdot \nabla X_k} \tag{5}$$

Reynolds Stress Equation

$$\frac{\partial \alpha_k \bar{\rho}_k \overline{v'_{k,i} v'_{k,j}}}{\partial t} + \frac{\partial \alpha_k \bar{\rho}_k \overline{v'_{k,i} v'_{k,j}} v'_{k,l}}{\partial x_l} = -\alpha_k \rho_k \overline{v'_{k,l} v'_{k,i}} \frac{\partial \overline{v}_{k,j}}{\partial x_l} - -\alpha_k \rho_k \overline{v'_{k,l} v'_{k,j}} \frac{\partial \overline{v}_{k,i}}{\partial x_l}$$

$$- \frac{\partial \alpha_k \rho_k \overline{v'_{k,i} v'_{k,j} v'_{k,l}}}{\partial x_l} - \left(\frac{\partial \alpha_k \overline{p'_k v'_{k,j}}}{\partial x_i} + \frac{\partial \alpha_k \overline{p'_k v'_{k,i}}}{\partial x_j} \right)$$

$$+ \alpha_k \overline{p'_k \left(\frac{\partial v'_{k,j}}{\partial x_i} + \frac{\partial v'_{k,i}}{\partial x_j} \right)} + \left(\frac{\partial \alpha_k \overline{\tau'_{k,il} v'_{k,j}}}{\partial x_l} + \frac{\partial \alpha_k \overline{\tau'_{k,jl} v'_{k,i}}}{\partial x_l} \right)$$

$$- \alpha_k \rho_k (\varepsilon_{k,ji} + \varepsilon_{k,ij}) + W'_{k,ji} + W'_{k,ij} + \overline{\rho v'_i v'_j (v_l - v_{li}) \frac{\partial X_k}{\partial x_l}} \tag{6}$$

where,

$$\varepsilon_{k,ij} = \frac{1}{\rho_k} \overline{\tau'_{k,il} \frac{\partial v'_{k,j}}{\partial x_l}} = \frac{1}{\alpha_k \rho_k} \overline{X_k \tau'_{il} \frac{\partial v'_j}{\partial x_l}} \tag{7}$$

and,

$$W'_{k,ij} = -\overline{v'_i T'_{jl} \frac{\partial X_k}{\partial x_l}}. \tag{8}$$

Taking the trace of equation (8) we obtain,

Turbulent Kinetic Energy Equation

$$\frac{\partial \alpha_k \rho_k \bar{k}_k}{\partial t} + \nabla \cdot \alpha_k \rho_k \bar{k}_k \bar{v}_k = -\alpha_k \rho_k \overline{v'_k v'_k} : \nabla \bar{v}_k - \nabla \cdot \alpha_k \rho_k \overline{\bar{k}_k v_k} - \nabla \cdot \alpha_k \overline{p'_k v_k}$$

$$+ \nabla \cdot \alpha_k \overline{\tau_k \cdot v'_k} - \alpha_k \rho_k \bar{\varepsilon}_k + W'_k + \overline{k_i (v - v_i) \cdot \nabla X_k} \tag{9}$$

Finally, we have the,

Turbulence Dissipation Equation

$$\frac{\partial \alpha_k \bar{\varepsilon}'_k}{\partial t} + \frac{\partial \alpha_k \bar{\varepsilon}'_k \overline{v'_{k,j}}}{\partial x_j} = -2\nu_k \alpha_k \frac{\partial \bar{v}_{k,i}}{\partial x_j} \left(\overline{\frac{\partial v'_{k,i}}{\partial x_l} \frac{\partial v'_{k,j}}{\partial x_l}} + \overline{\frac{\partial v'_{k,l}}{\partial x_i} \frac{\partial v'_{k,l}}{\partial x_j}} \right) - 2\nu_k \alpha_k \overline{v'_{k,j} \frac{\partial v'_{k,i}}{\partial x_l} \frac{\partial^2 \bar{v}_{k,i}}{\partial x_l \partial x_j}}$$

$$- 2\nu_k \alpha_k \overline{\frac{\partial v'_{k,j}}{\partial x_l} \frac{\partial v'_{k,i}}{\partial x_l} \frac{\partial v'_{k,i}}{\partial x_j}} - 2\nu_k^2 \alpha_k \overline{\left(\frac{\partial^2 \bar{v}_{k,i}}{\partial x_l \partial x_j} \right)^2} - 2\frac{\nu_k}{\rho_k} \frac{\partial}{\partial x_i} \left(\alpha_k \overline{\frac{\partial v'_{k,i}}{\partial x_l} \frac{\partial p'_k}{\partial x_l}} \right)$$

$$- \frac{\partial \alpha_k \overline{\varepsilon'_k v'_{k,j}}}{\partial x_j} + \nu_k \frac{\partial^2}{\partial x_j^2} \left(\alpha_k \bar{\varepsilon}'_k \right) + D_k$$

$$\tag{10}$$

where,

$$\varepsilon' = \nu \overline{\frac{\partial v'_i}{\partial x_l} \frac{\partial v'_i}{\partial x_l}} \tag{11}$$

$$D_k = 2\frac{\nu}{\rho} \overline{\left(\frac{\partial v'_i}{\partial x_l} \frac{\partial p'}{\partial x_l} \right) \frac{\partial X_k}{\partial x_i}} - \nu \overline{\frac{\partial}{\partial x_j} \left(\varepsilon' \frac{\partial X_k}{\partial x_j} \right)} - \nu \overline{\frac{\partial \varepsilon'}{\partial x_j} \frac{\partial X_k}{\partial x_j}} \tag{12}$$

$$+ 2\nu v'_i \overline{\frac{\partial X_k}{\partial x_l}} \left(\frac{\partial \bar{v}_{k,i}}{\partial t} + \bar{v}_{k,j} \frac{\partial \bar{v}_{k,i}}{\partial x_j} + \frac{1}{\rho_k} \frac{\partial \bar{p}_k}{\partial x_i} - \frac{\partial^2 \bar{v}_{k,i}}{\partial x_l \partial x_l} - g_i \right) + 2\nu \frac{1}{\rho} p' \overline{\frac{\partial X_k}{\partial x_l} \frac{\partial}{\partial x_l} \left(\frac{\partial \bar{v}_i}{\partial x_i} \right)}$$

2.2 Closure

2.2.1 The interfacial momentum source

The interfacial momentum source can be partitioned into drag and non-drag components [Lahey & Drew, 1990], as.

$$\mathbf{M}_k = \overline{-\mathbf{T} \cdot \nabla X_k} = \mathbf{M}_k^{(D)} + \mathbf{M}_k^{(ND)} \tag{13}$$

For drag we may assume:

$$\mathbf{M}_c^{(D)} = -\mathbf{M}_d^{(D)} = \frac{1}{8} \rho_c C_D |\mathbf{v}_r| \mathbf{v}_r A_i''' \tag{14}$$

The non-drag component may be obtained assuming inviscid flow around spherical particles [Arnold, 1988; Park, 1992]. The average quantities were obtained using cell-averaging techniques [Nigmatulin, 1979], which are an approximation to ensemble averaging. The resulting expression includes virtual mass effects and a lateral force induced by the non-uniform flow field around a spherical particle. The latter force is called lift force and is given by [Drew & Lahey 1987; 1990]:

$$\mathbf{M}_c^L = C_L \varepsilon_d \rho_c \overline{\mathbf{v}}_r \times \nabla \times \overline{\mathbf{v}}_c \tag{15}$$

The effects of the liquid turbulence interaction with particles/bubbles are included in the turbulent dispersion force:

$$\mathbf{M}_c^{(ND),TD} = -\mathbf{M}_d^{(ND),TD} = C_{TD} \rho_c k_c \nabla \alpha_d \tag{16}$$

2.2.2 Binary Collisions between the particles and the particle-wall collisions

Alajbegovic [1994] has developed closure laws for the stress induced in the dispersed phase and the transfer of the kinetic energy. For brevity only the procedure used to derive the expressions is described here. The following assumptions were made: collisions between more

than two particles at the same instant are negligible; all collisions are elastic with negligible rotational effects. Starting from the expression for the average stress inside the dispersed phase given by Bachelor, [1970] an integral expression for the collision-induced shear stress is obtained by evaluating the probabilities of collisions of particles moving with given velocity, position and size. This expression is similar to that obtained by Chapman and Cowling [1970]. This was further integrated to obtain the final expressions. Similar procedure was used to calculate particle-wall collision-induced force.

2.2.3 Turbulent Interfacial Work

The interaction between the dispersed particles and the eddies is governed by the following equations:

$$\frac{dv'_{p,i}}{dt} = -\frac{1}{\tau_R} (v'_{p,i} - v'_{c,i})$$ (17)

$$\frac{d}{dt} (m_c v'_c + m_p v'_p) = 0$$ (18)

The interfacial work due to particle interactions with the continuous phase turbulence is:

$$W'_{d,ij} = \frac{\rho \alpha}{\tau_R} \left(C_1^W \overline{v'_{c,i} v'_{c,j}} - C_2^W \overline{v'_{p0,i} v'_{p0,j}} \right)$$ (19)

where,

$$\tau_R = \frac{4\rho_d}{3\rho_c} \frac{D_p}{C_D |\bar{v}_p - \bar{v}_c|}$$ (20)

2.2.4 Algebraic Stress model for the dispersed phase Reynolds Stress

Starting with the assumption that:

$$\frac{\overline{v'_i v'_j}}{k} \cong \text{const.}$$ (21)

it can be shown that:

$$\overline{v'_{d,i} v'_{d,j}} = \frac{k_d \overline{v'_{c,i} v'_{c,j}} - \dfrac{k_d \tau_R}{\alpha_d 2A}\left(\overline{v'_{d,l} v'_{d,i}}\dfrac{\partial \bar{v}_{d,j}}{\partial x_l} + \overline{v'_{d,l} v'_{d,j}}\dfrac{\partial \bar{v}_{d,i}}{\partial x_l} - K_{ij} \right)}{\bar{k}_c - \dfrac{\tau_R}{\alpha_d 2A}\left(\overline{v'_{d,l} v'_{d,i}}\dfrac{\partial \bar{v}_{d,i}}{\partial x_l} - K_l \right)} \tag{22}$$

In case of negligible collisions and small gradients in the dispersed phase's mean velocity, the above equation reduces to:

$$\overline{v'_{d,i} v'_{d,j}} = C_{R,ij}\frac{k_d}{\bar{k}_c}\overline{v'_{c,i} v'_{c,j}} \tag{23}$$

The above models have been tested against experimental data obtained at Rensselaer and elsewhere for various flow situations, and show remarkable accuracy.

3.0 Solid/Liquid Experiments

In a two-phase mixture for low volume fractions, the lift force is one of the most important phenomena affecting the radial distribution of the flow. This effect is due to the relative velocity between the two phases. Serizawa et. al. [1988] demonstrated that this lift force pushes bubbles towards the wall in upward flows and towards the center of the conduit for downward flows.

Figure-1 shows how the gravity affects the hydrodynamic behavior of a turbulent two-phase flow. We may eliminate the buoyancy force by using a dispersed phase of same density as that of continuous phase. Assad et. al. [1995] measured the liquid and dispersed phase distribution in a solid/liquid two-phase flow in a horizontal pipe using a Laser Doppler Anemometer (LDA). The dispersed phase consisted of ~2.0 mm average diameter size expanded polystyrene particles with specific gravity of 1.03. The test section was 30.6 mm in diameter and the pipe was made out of a special optically clear material (FEP, Fluorinated Ethylene Propylene) with the same index of

refraction as water. Measurements for the velocity profile, turbulent structure and the volume fraction for each phase were made for various flow rates and global volume fractions.
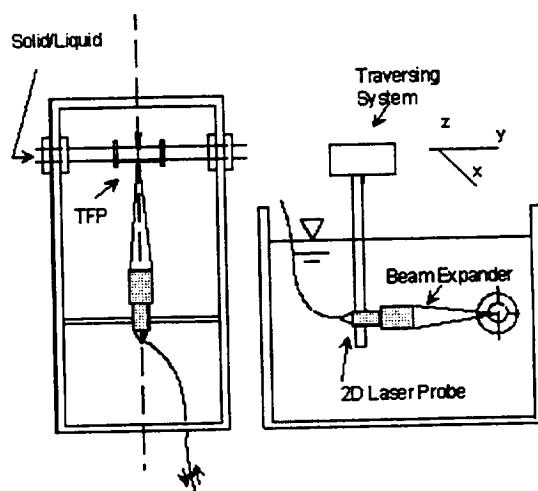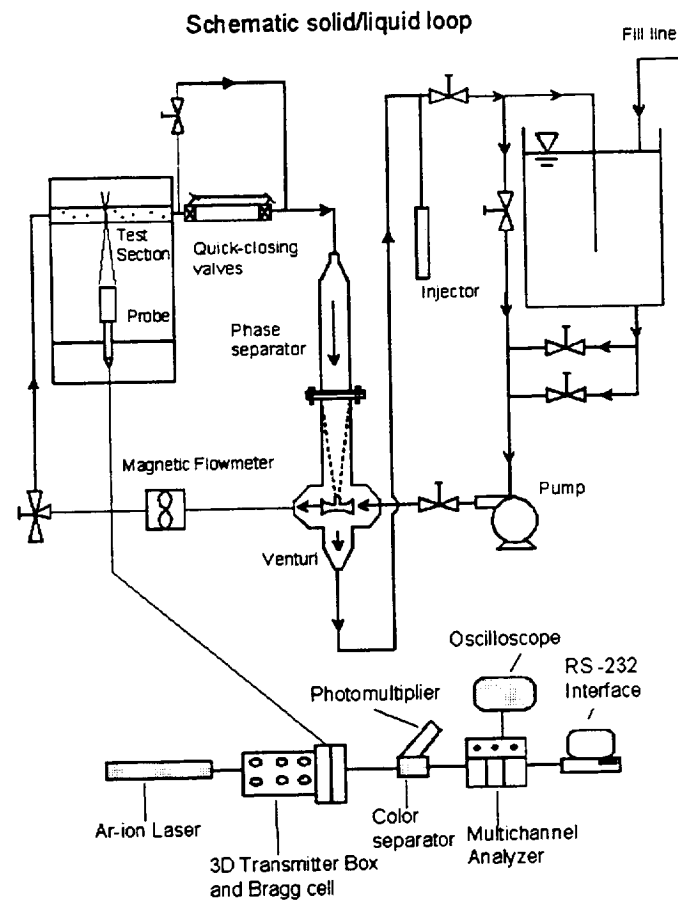
Figure-2 shows the schematic of the experimental facility used to make the measurements. Water recirculated through the loop in continuous mode. A specially designed phase separator did not allow the particles to go through the pump where they could be damaged. Figure-3 shows the details of the phase separator. The phase separator has three principal components: a large diameter tank, a venturi and a porous funnel i.e., screen. Water coming out of the pump goes through the venturi creating a low pressure at the throat. This aspirates the particles into the stream coming into the funnel from the loop. Thus flow coming out of the venturi carries with it all the particles, while the funnel lets the loop water go to the pump inlet. The purpose of the large diameter tank is to slow down the flow coming into the funnel. This arrangement makes sure that same global void fraction is maintained at all times.

To have a check on the LDA measurements, a quick closing valve was used to measure the global void fraction. A calibration was done to have precise information about the volume of the pipe. A calibrated glass tube was used to measure the volume of the particles once they were removed from the quick closing valve. After 12 measurements for each flow rate, the mean statistical error was around 2.4%; thus the average of 12 measurements was appropriate to determine the global fraction of particles.
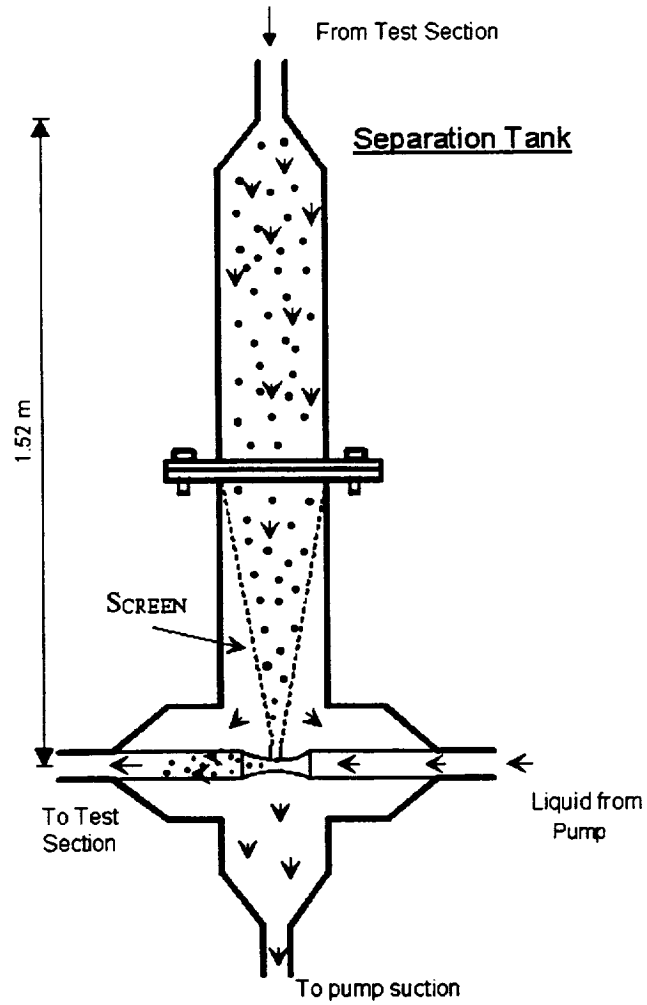
The two-fluid model described above was incorporated into the PHOENICS code to test it against the data for neutrally buoyant particles. Although the model was developed for vertical flows, only, the neutral buoyant particle data for horizontal flows can still be compared against the calculations. Figures-4 and 5 show that the agreement with data is good.
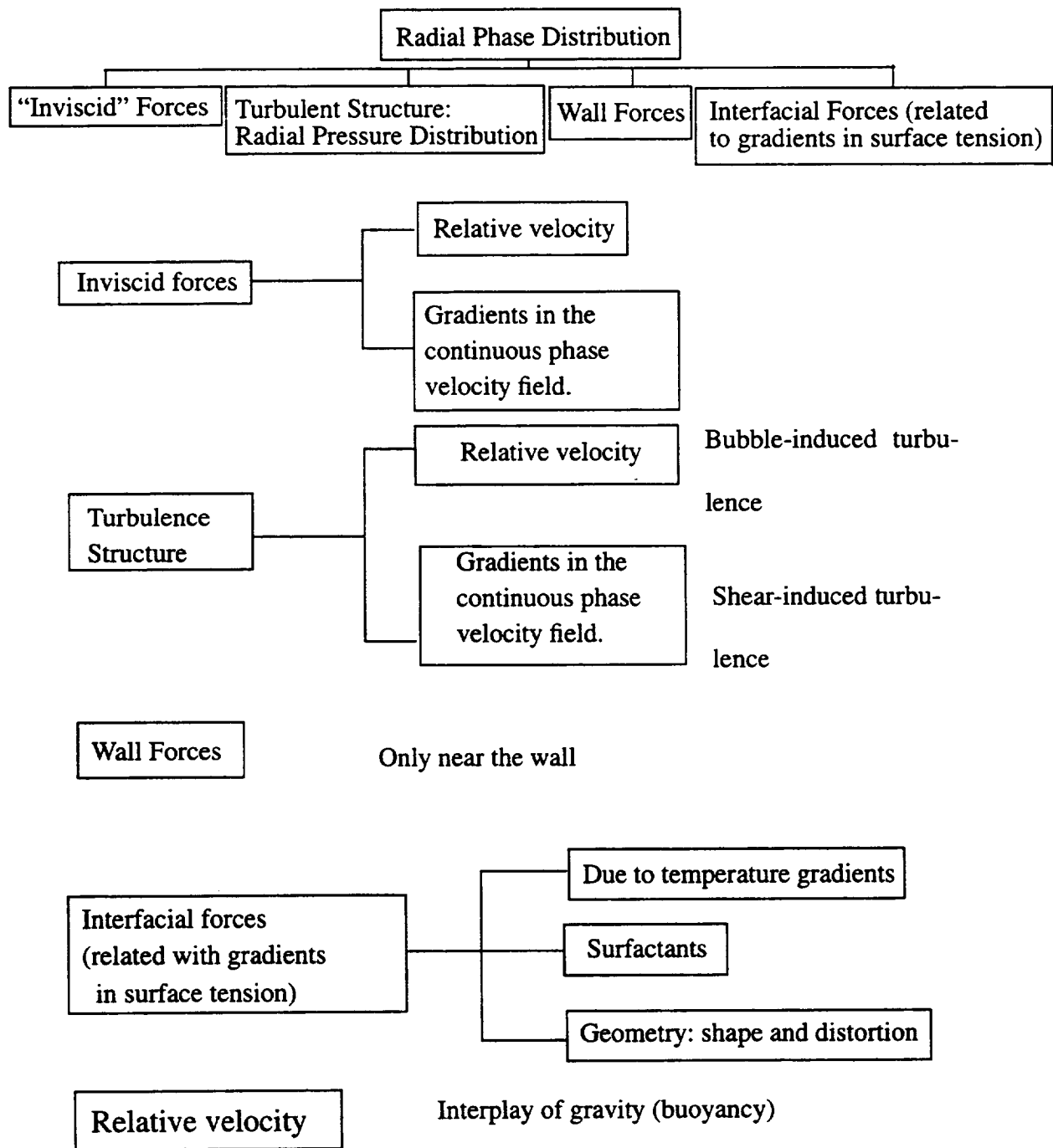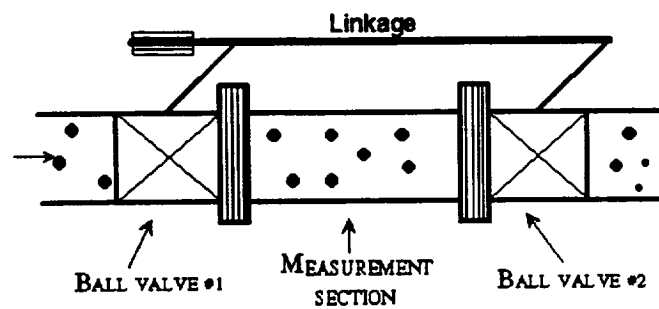
FIGURE 1. Parametric dependence of two-fluid models

FIGURE 2. Schematic of the solid/liquid experimental facility

From Test Section

Separation Tank

1.52 m

SCREEN

To Test Section

Liquid from Pump

To pump suction

For Horizontal Experiments

Linkage

BALL VALVE #1

MEASUREMENT SECTION

BALL VALVE #2

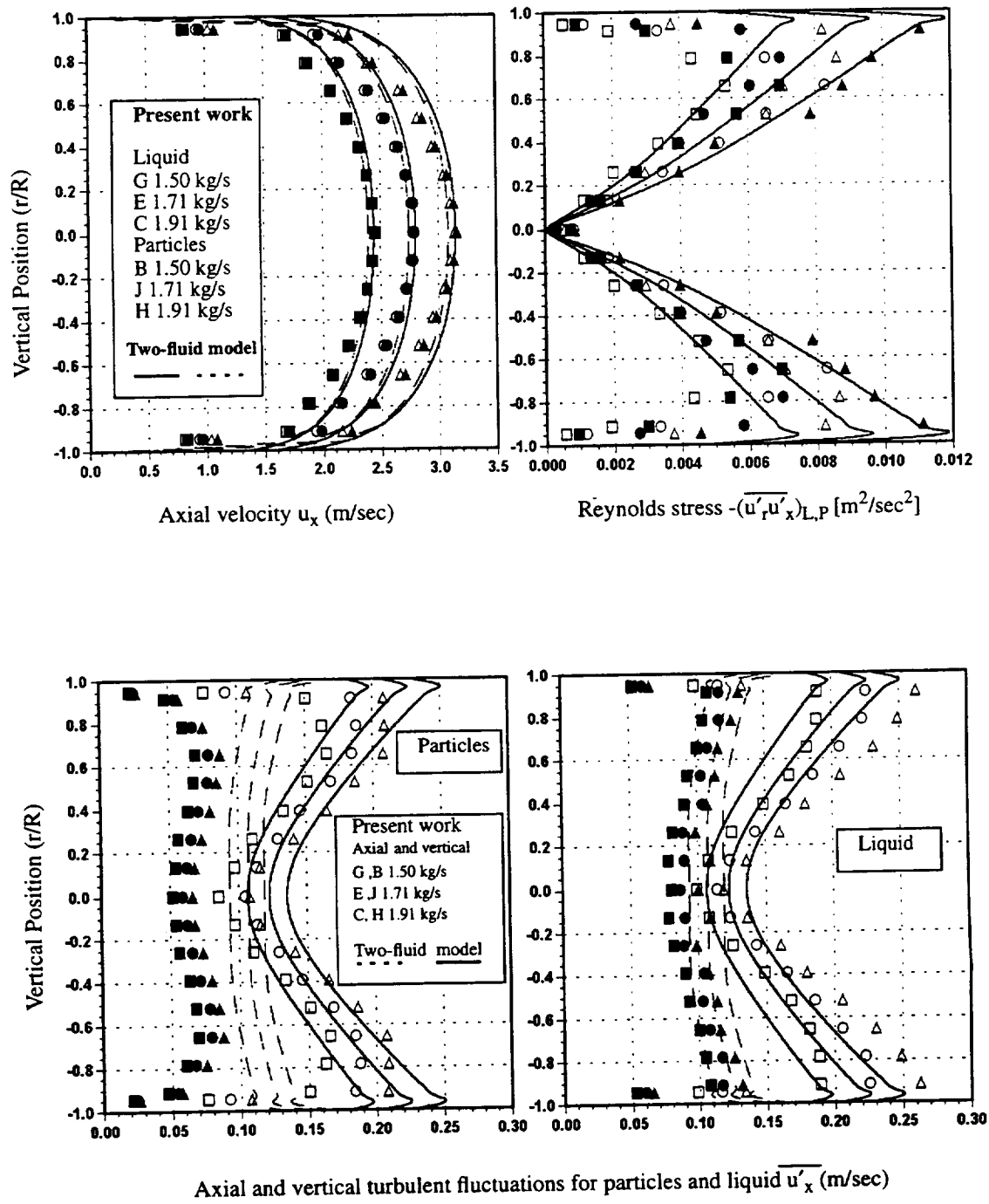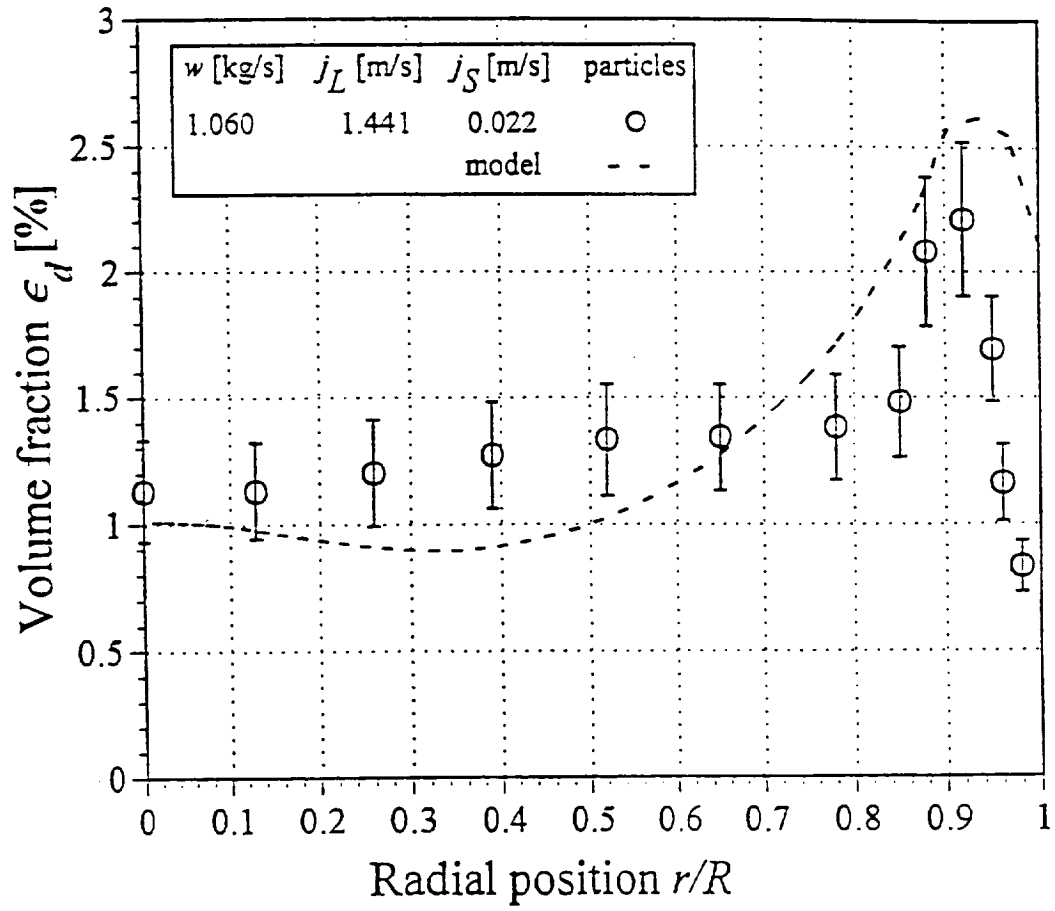**FIGURE 3. Details of the phase separator and quick closing valve**

FIGURE 4. Comparison between measured and predicted velocity and turbulence quantities for neutral particles.

FIGURE 5. Comparison between the predicted and measured volume fraction profiles for neutral buoyant particles.

4.0 Liquid/Liquid Experiments

The particles which were used by Assad [1995] were solid spheres with a non-deformable, non-slip interface. The flow dynamics around them are well understand and documented. In case of bubbles and droplets, there is no solid interface; the fluid outside interacts with the fluid inside giving rise to internal circulations and deformations. Pressure differentials can deform the surface so that they are no longer spherical. All this affect the interfacial momentum transfer and the turbulence structure in a significant way. However, if the droplets/bubbles are small enough, the deformations is very small compared to their size and hence can be neglected. The liquid/liquid experiments allow us to further verify our models and collect data to guide us in further enhancements.

4.1 Summary of the work done earlier

The experimental facility and the measurement strategies have evolved from a closed-loop, in-line oil separation mode to a batch mode with an oil droplet injector. Experience with the components involved has guided us to improve the facility to have a better control over the parameters involved.

Our search for a cost effective immiscible oil with same density as water at room temperature led us to silicon oil and n-butyl benzoate as the dispersed phase. Thus, microgravity conditions are simulated by matching the two densities closely, thus eliminating the buoyancy force. The properties of these are well documented in various property tables. Butyl benzoate has a specific gravity of 1.0 at 20° C. Another property which is of concern is the change in density with temperature. Butyl benzoate is more sensitive to temperature as compared to water. This is extremely useful for separating the two fluids. Thus, by heating the mixture collected and elevat-

ing the temperature by 20°C the difference in density of the two fluids makes it possible to gravity separate them. Also, butyl benzoate has a refractive index of 1.494 for which is good for LDA measurement purposes and is 3.59 times more viscous than water. It has since been shown to have satisfactory optical properties for Phase Doppler measurements. As a consequence butyl benzoate will be used in out experiments.

Initially, our test facility consisted of a oil/water closed loop in which both the oil and water were allowed to go through the pump. In one of the typical data sets, the mean diameter of the droplets was found to be 181 microns while the range of sizes present was from 40 microns to 600 microns. A few large droplets of oil were also detected with sizes between 1.2 mm to 1.4 mm. Unfortunately, after a period of time the pump formed an emulsion out of the mixture. Clearly, the closed loop mode of operation was not suitable for obtaining mono-dispersed droplet flows. This motivated us to consider open loop operation with an injector to produce a mono-dispersed suspension.

A droplet injector was designed and has been constructed with the following characteristics: (i) ability to control the flow rate of water, (ii) ability to control the diameter of the oil droplets, (iii) ability to control the relative flow rates of water and oil to obtain desired global void fraction, and (iv) most importantly, the droplet size distribution should be as small as possible. Indeed, we want a mono-dispersed flow so that a correlation between the size of the droplet and the phase distribution phenomenon may be established. The obvious choice to achieve the above objectives is to have capillary tubes as injection units. Initially it was not clear whether the last requirement above could be met or not and whether we can predict the size of the droplets being formed if size of the tubes is known. A preliminary calculation was done to predict the size of the droplets as a function of oil volume flow rate, velocity of the stream trying to shear off the drop-

lets from the tips and the size of the capillary. This was guided by the work done by several researchers [Hayworth et. al., 1950; Null et. al., 1958] where a balance between the drag on the spherical droplet being formed at the tip due to the fluid motion and the cohesion forces due to surface tension yielded a correlation between the droplet size form and the capillary size with fluid velocity as a parameter. This droplet injector has been tested and appears to be functioning as predicted.

The separation of oil from water will be accomplished by heating the mixture to 40°C and then, as described earlier, the oil floats to the top where it can be decanted off. If any traces are still left, they can be separated with a dedicated centrifuge unit. In-line separation processes were extensively explored without finding any feasible option. The batch options turns out to be convenient enough with a down time of a couple of hours between two runs which can be utilized for processing data and preparing for the next run.

Some data was obtained for single-phase and two-phase flows for various Reynolds number to give us an idea of trends to be expected and to fine tune the instrumentation involved. No notable difference was observed between the two-phase data and the single-phase data because the droplets were very small in size. During these tests, LDA data was found to be inadequate to estimate the size of the droplets accurately. This inadequacy stems from the method of interpreting the transit time of a burst as an indicator of the size of the droplets. This mode of droplet size estimation can only be used to get an approximate idea of the size distribution. For more accurate data we may use a Fiber Phase Doppler Anemometer (FPDA) which relies on the phase difference between the reflected light detected by two detectors, a fixed distance apart, to determine the size of the droplet.

An additional limitation of the facility was encountered when the FPDA was used to obtain size and velocity data. To obtain data, the transmitting and receiving probe's measuring volumes must coincide at all locations while traversing. It was realized that if alignment is made at one point then it is impossible to traverse to another location without loosing the alignment. This happens because of the differential change in the optical path of the signal to the receiving probe. This can be solved by using a FEP conduit and submerging both the probes under water so that the optical path length does not change when traverses are made.

As described above all the subtasks mentioned in the previous report have been accomplished. Now the work is in progress is focussed on acquiring the actual data.

4.2 Work done since the last report

4.2.1 The oil-water loop

As described in the previous report a batch mode oil/water loop has been built and tested. The schematic of the loop is shown in figure-6. To summarize, this design was decided upon because of two reasons:

(1) We could not find a viable in-line full flow separation process for neutral buoyant oil in water. Rather, separation will be done in batches by heating the mixture followed by gravity separation.

(2) To avoid the realignment of the FPDA probe at each measurement location. In the current facility the probes and the FEP test section are all immersed in water so that no correction or alignment has to be done for measurements at different locations.

4.2.2 The oil/droplet injector

The oil droplet injector was tested to find out the effect of oil and water flow rates on the size distribution of droplets. A small test loop was constructed outside of the main test facility for ease of observation and control. Figure-7 shows a schematic of this facility. Two methods were used to measure the droplet size distribution. The first method used was to collect the droplets in a glass petridish and estimate the size of the droplets by placing them on graph paper. The results have been recorded with a CCD camera for future reference. The drawback of this method was that the droplets coalesced in a short time. Also the collection process itself affects the droplets. The second method was to take pictures of the droplets as they passed through the box with windows. These two methods combined to give us a good indication of the injector performance. Following conclusions were drawn from the data obtained:

(1) The droplet size decreases with an increase in water flow rate.

(2) The average droplet size increases with the increase in oil flow rate and at the same time the spread in the size distribution increases.

Figure-8 shows a selection of photographs taken for the droplets.

### 4.2.3 Optimization of the FPDA for the oil/water mixtures

A study was done to verify that an FPDA can measure oil droplet size. This was necessary to optimize the setup variables and verify the optical properties of oil in the context of the FPDA measurements. Figure-9 below shows the experimental facility used for this purpose. A small glass tank was filled with a known amount of water. It was determined that the reflection mode of diameter measurement is most suited for actual measurements. The power of the laser in all cases was kept low (~200 mW). Also the vertical component of velocity was small. These are certainly

not the best settings but once the system has been optimized at these settings then the scaling the experiment to faster velocities and higher power will not be difficult and should result in large improvements. This experiment was done in three stages. Stage one consisted of alignment and measurement of particle sizes and velocity, using glass bubbles as seeding. This constitutes the optimum case to start with because of the large relative refractive index of glass with respect to water. Stage two consisted of redoing the work of stage one but without any glass seeding. The third and final stage consisted of adding oil into the tank with increasing global void fractions. Two void fractions were measured: 0.07% and 0.21%. Larger void fractions could not be tried because of the formation of an emulsion by the stirrer. This increased the turbidity of the mixture to such a large extent that the measurement rate decreased by a factor of 10. Table 2 below shows the data obtained. Runs a01 through a04 are tests with glass seedings, a05 through a07 were without any seeding, a08 with a 0.07% volume fraction of oil and a09 with 0.21% volume fraction of oil. As indicated earlier the velocities involved were very small and it was observed that even a small increase in the velocity resulted in a very large increase in the acceptance rates.

Figure-10 shows the seeding size distribution in which 3.5 cc of the seeding was used to seed 19.6 liters of water. A sample of the seeding was analyzed under a travelling microscope to determine the sizes present. The glass seeding sizes were found to be in the range 5 μm to 100 μm, with most of them in 25 to 50 μm range. Although the data is not statistically representative of the distribution, it gave us the bounds on size. The histogram in figure-10 is accurate to that extent with most particles the same range as above. Optimization of the alignment and different parameters led to different trials with most of them resulting in the similar distribution. The best settings correspond to trial number 11 in the a04 series.

Figure-11 shows the particle size distribution in unseeded water. The particles measured are the natural seeding suspended in the water supply. Most of the particles are in range 0 to 20 μm. Figure 12 shows the oil droplet size distribution for a volume fraction of 0.07%. Immediately after the measurements were done with unseeded water, 15.5 cc of oil was added. The stirrer immediately broke up the oil globules into small droplets and a delay of about 10 minutes was allowed before measuring to allow the system to stabilize. The histogram in figure-12 shows the range of sizes present is 0 to 340 μm. Most of the particles are below 100 μm in diameter. If this is compared with the figure-11, it is practically impossible to say which of the data belong to the droplets and which to the natural seeding especially in the 0-25 μm range. This is the case with low volume fraction, however at higher volume fraction, the data percentage in this range must be small to be able to neglect the influence of natural seeding. This was confirmed by adding more oil to the tank, the resulting void fraction being 0.2%. Figure-13 shows a typical data set obtained at this volume fraction. Here most of the droplets are in range 40 to 100 μm and the fraction of particles/droplets less than 20 μm is very small. With the injector in the main loop, we should be able to keep the global void fraction relatively large enough without any emulsification. Thus we are confident that with large sample sizes, the data will be representative of the true droplet size distribution.
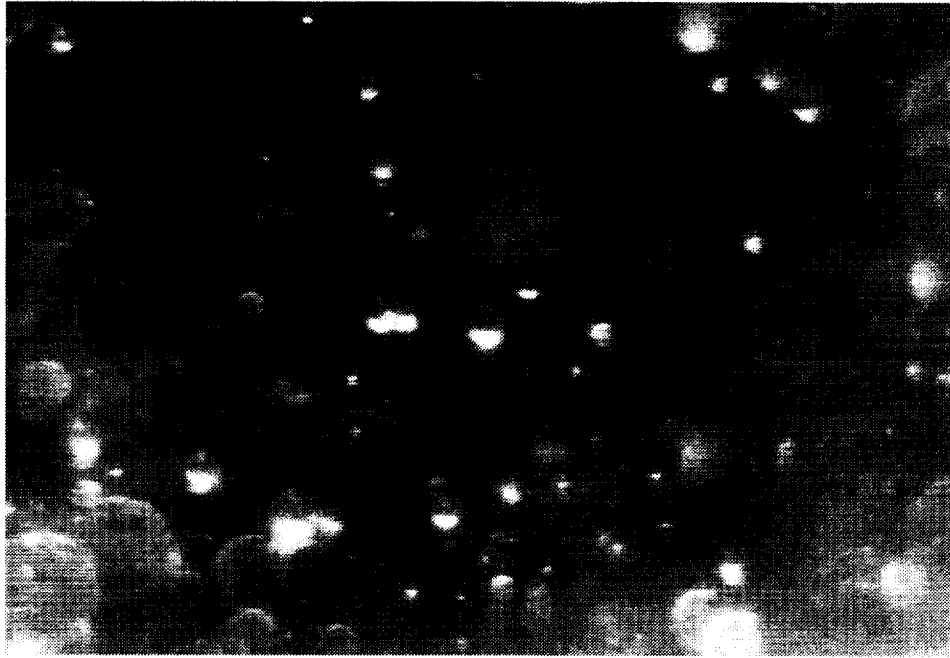
Interfacial area is a quantity of interest for estimating the interfacial mass, momentum and energy transfer. Figures 14 and 15 show the same information as in figures 10 through 13 in terms of interfacial area.
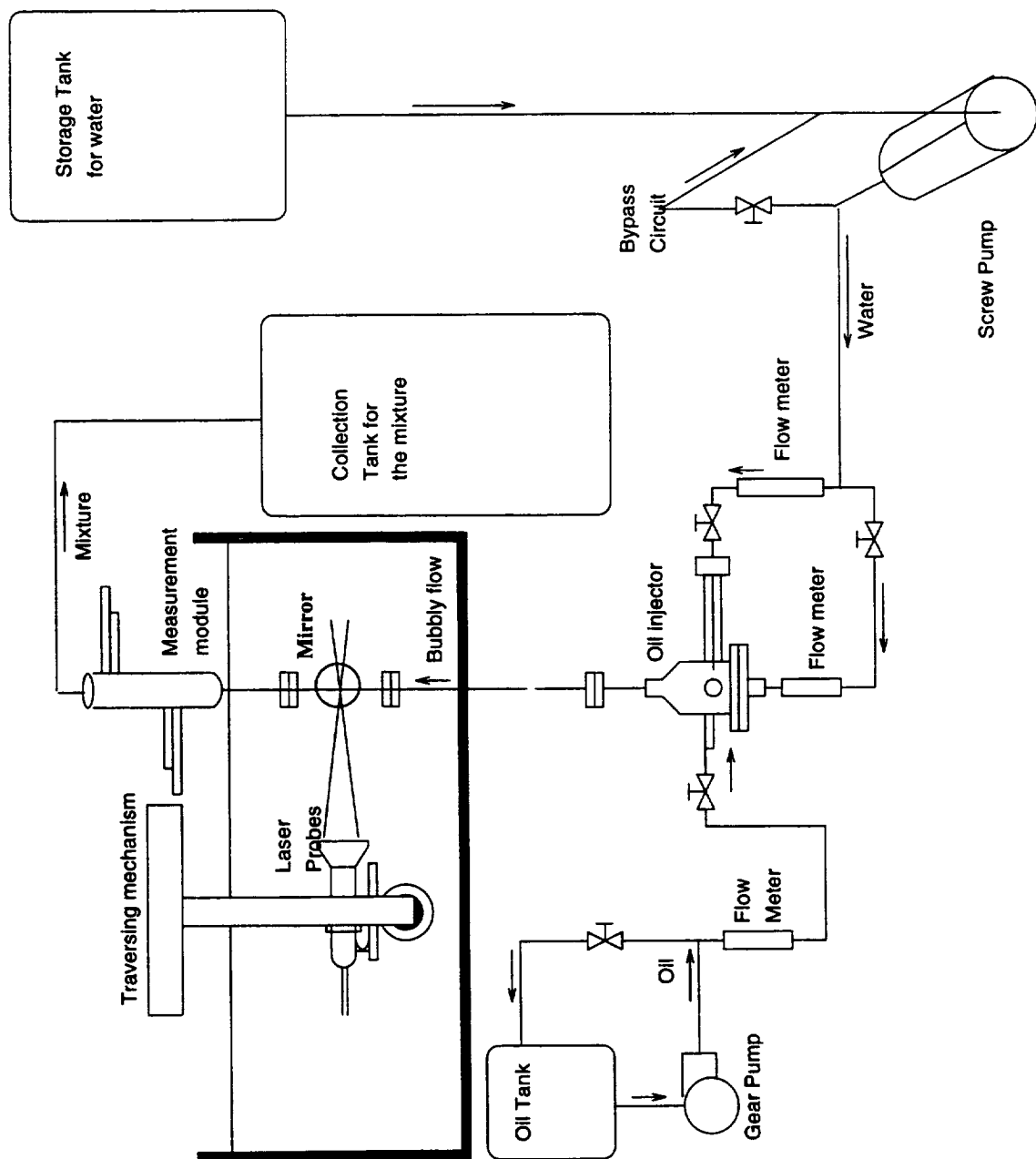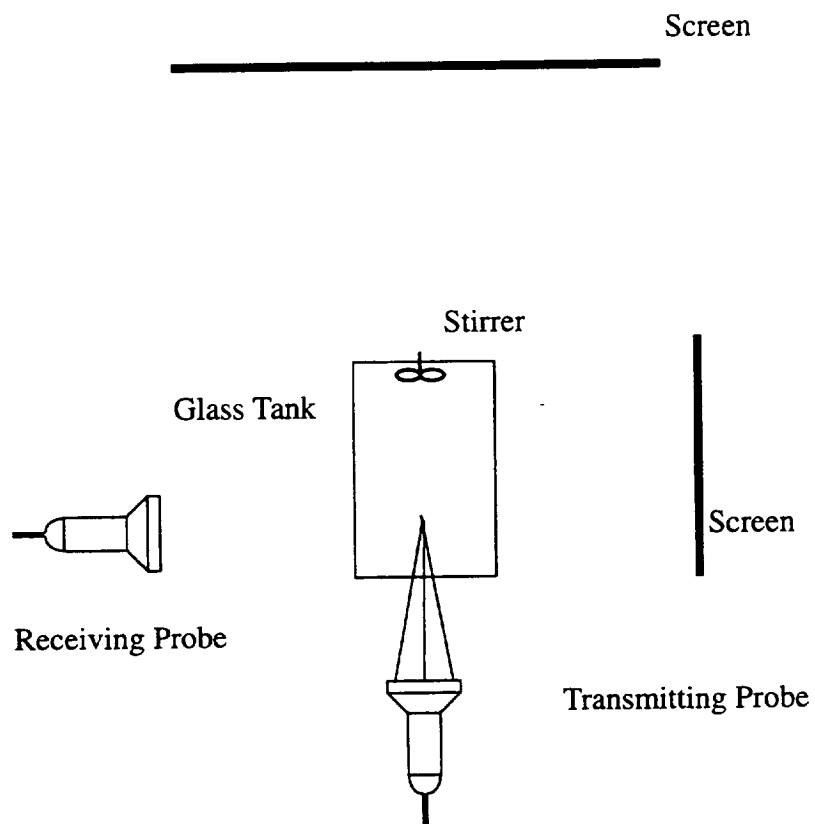
FIGURE 6. Schematic of the new facility.
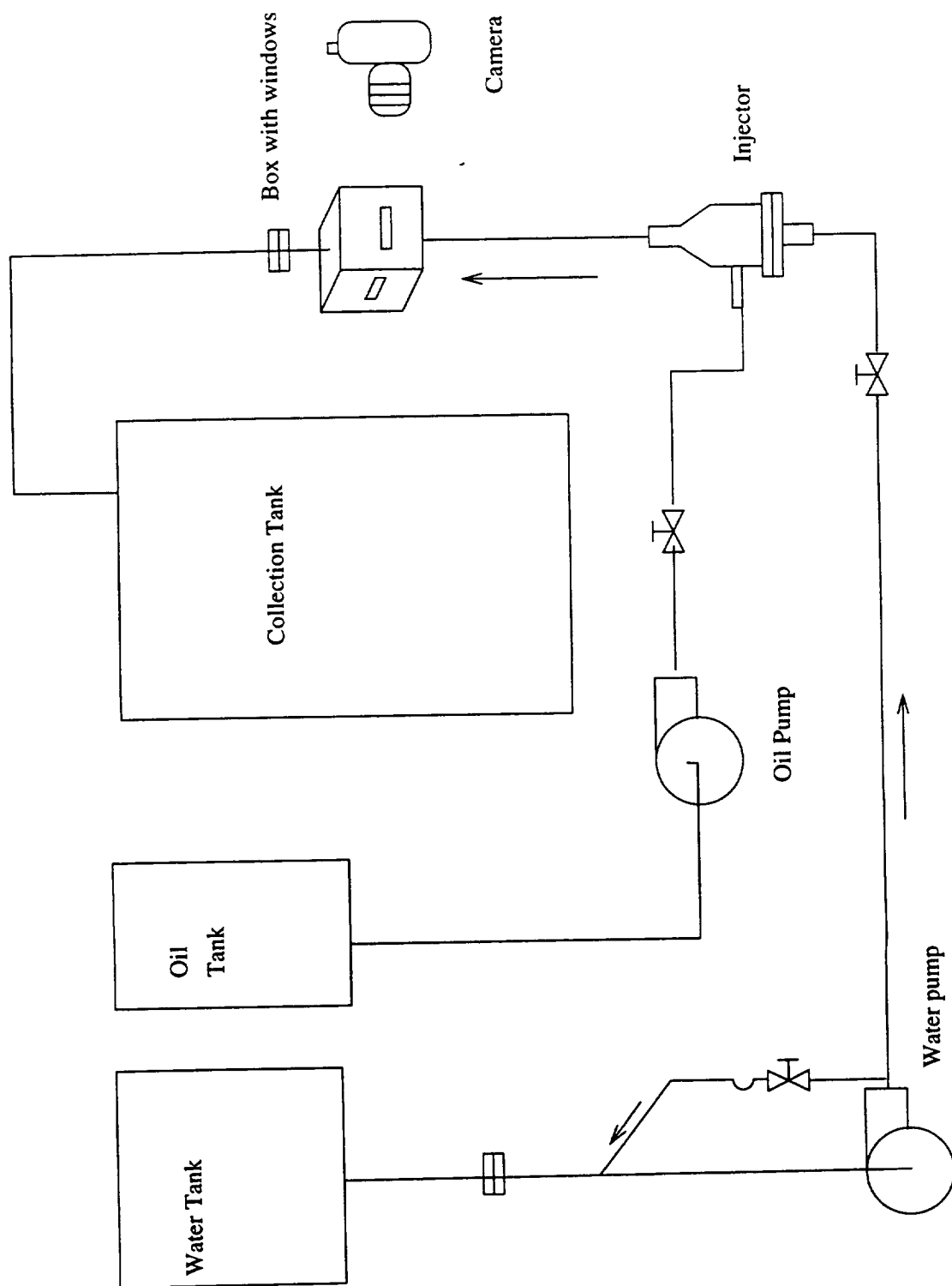
FIGURE 7. Schematic of the oil-droplet injector test loop.

FIGURE 8. Photographs with oil droplets, magnification=5.34

FIGURE 9. Schematic of the FPDA trial setup

Table 2: Data from the FPDA trials

File Name	Trial No.	U$_{mean}$ (cm/s)	Void Fraction	D$_{mean}$ (μm)	Validated Samples	% Acceptance	Data Rate (Hz)	Elapsed Time (sec)
a01.dat	1.	.166	.103	-	390.	32.5	.6	654.35
a02.dat	1.	.419	.175	-	500.	27.6	1.0	525.75
a03.dat	1.	.330	2.149	-	2000.	78.8	6.9	290.27
a04.dat	1.	.762	.376	31	250.	21.7	1.8	138.66
a04.dat	2.	1.185	.434	33	250.	24.5	2.1	118.88
a04.dat	3.	1.237	.103	49	250.	7.8	.6	435.47
a04.dat	4.	.737	.357	29	250.	20.9	1.7	149.90
a04.dat	5.	.942	.321	32	250.	17.2	1.6	158.04
a04.dat	6.	1.040	.328	37	250.	19.5	1.7	150.24
a04.dat	7.	1.021	.302	36	250.	18.7	1.5	167.54
a04.dat	8.	.663	.263	30	250.	15.9	1.3	198.25
a04.dat	9.	1.225	.236	30	250.	21.1	1.1	224.34
a04.dat	10.	1.580	.122	11	35.	10.4	.7	52.42
a04.dat	11.	1.180	.284	29	250.	16.6	1.4	176.09
a04.dat	12.	1.289	.230	36	250.	12.9	1.2	216.08
a04.dat	13.	1.763	.177	25	250.	9.5	.9	270.24
a04.dat	14.	1.173	.048	23	14.	2.0	.2	62.50
a05.dat	1.	-.789	.281	62	38.	4.8	.5	76.50
a06.dat	1.	-.561	.125	52	174.	4.4	.4	387.85
a06.dat	2.	.450	.234	37	254.	11.9	1.0	261.15
a06.dat	3.	.238	.232	68	187.	12.8	1.1	171.37
a06.dat	4.	-.173	.284	58	157.	14.2	1.2	136.25
a06.dat	5.	.524	.182	105	80.	8.7	.8	104.10
a06.dat	6.	-.580	.150	14	23.	6.0	.6	37.16
a06.dat	7.	.289	.166	11	51.	8.9	.8	67.01

Table 2: Data from the FPDA trials

| File Name	Trial No.	U_{mean} (cm/s)	Void Fraction	D_{mean} (μm)	Validated Samples	% Acceptance	Data Rate (Hz)	Elapsed Time (sec)
a06.dat	8.	1.542	.016	11	6.	.9	.1	84.54
a06.dat	9.	-1.361	.051	11	15.	2.2	.2	87.00
a06.dat	10.	-.377	.187	48	49.	7.6	.8	59.53
a07.dat	1.	.984	.182	101	83.	9.4	.6	145.87
a07.dat	2.	.402	.258	148	37.	10.0	.6	63.90
a08.dat	1.	.321	.088	18	45.	4.7	.3	135.65
a08.dat	2.	.286	.191	76	129.	9.3	.6	224.69
a08.dat	3.	1.142	.185	84	64.	10.5	.5	121.21
a08.dat	4.	3.115	.322	110	179.	15.4	.9	194.60
a08.dat	5.	2.991	.464	122	119.	21.1	1.2	101.97
a08.dat	6.	3.538	.533	90	256.	26.3	1.6	155.78
a08.dat	7.	3.685	.567	130	262.	26.1	1.9	135.23
a08.dat	8.	3.371	.726	108	260.	33.6	2.4	107.73
a08.dat	9.	2.967	.652	121	174.	30.6	2.2	79.55
a08.dat	10.	4.479	.741	113	259.	30.8	2.5	102.26
a08.dat	11.	4.069	.757	116	259.	30.3	2.3	110.83
a08.dat	12.	3.583	.863	111	258.	30.8	2.5	102.19
a08.dat	13.	3.977	1.511	112	261.	15.3	4.6	56.45
a08.dat	14.	4.246	1.512	112	260.	26.2	4.6	56.75
a08.dat	15.	3.698	1.811	136	264.	23.1	5.0	52.97
a09.dat	1.	4.143	.475	164	262.	20.2	1.8	145.64
a09.dat	2.	3.701	.381	225	275.	19.5	1.7	162.98
a09.dat	3.	3.779	.286	255	276.	16.0	1.2	238.02
a09.dat	4.	3.618	.201	243	275.	13.6	.8	328.21
a09.dat	5.	3.381	.179	244	275.	12.8	.8	355.87
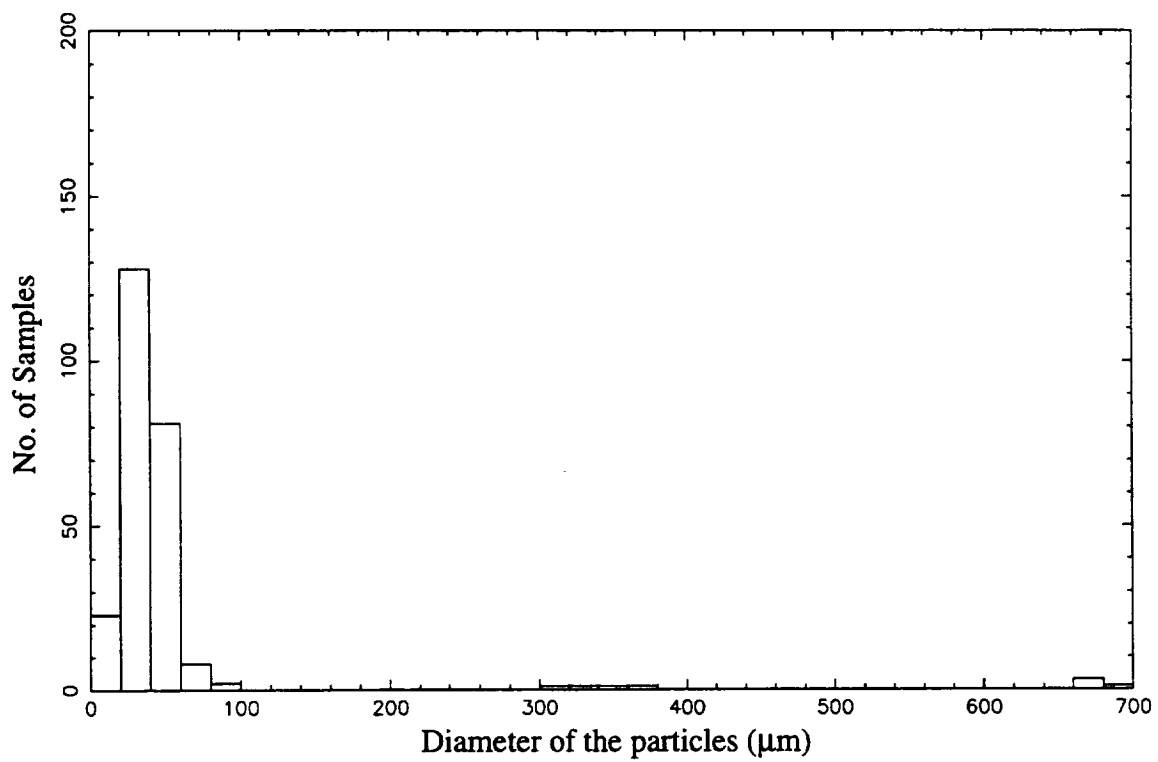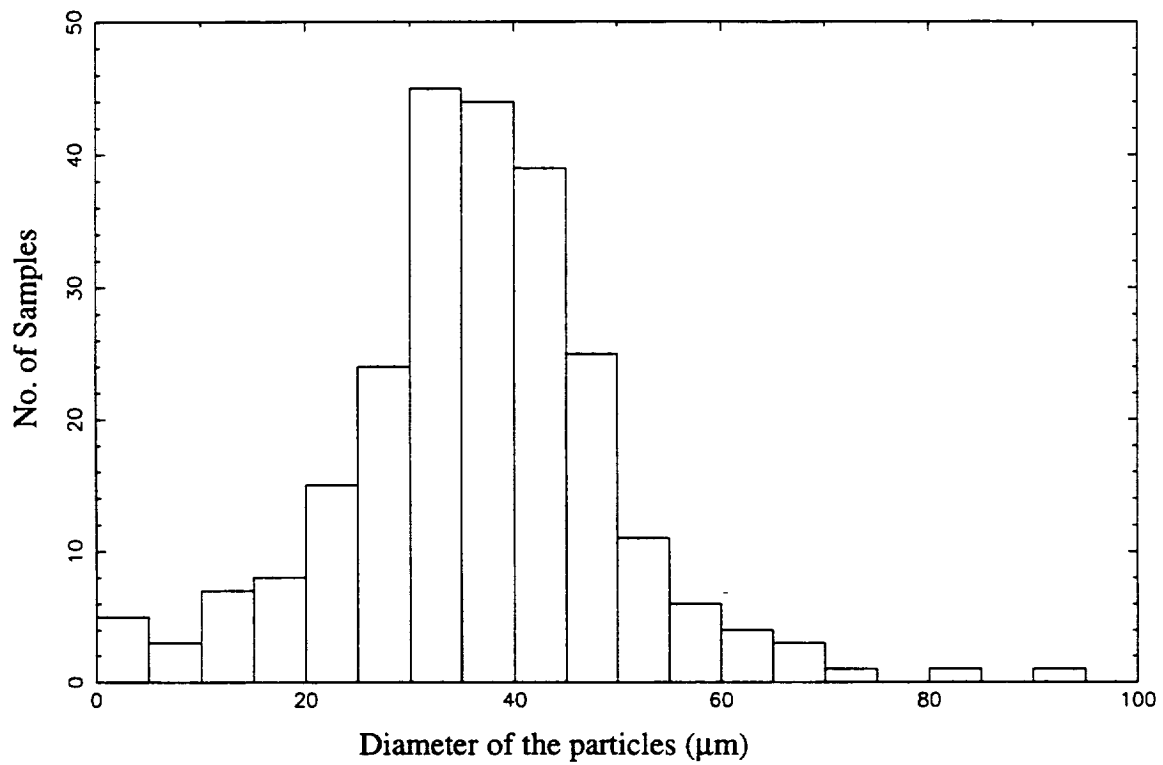
FIGURE 10. Typical particle size distribution with glass seeding
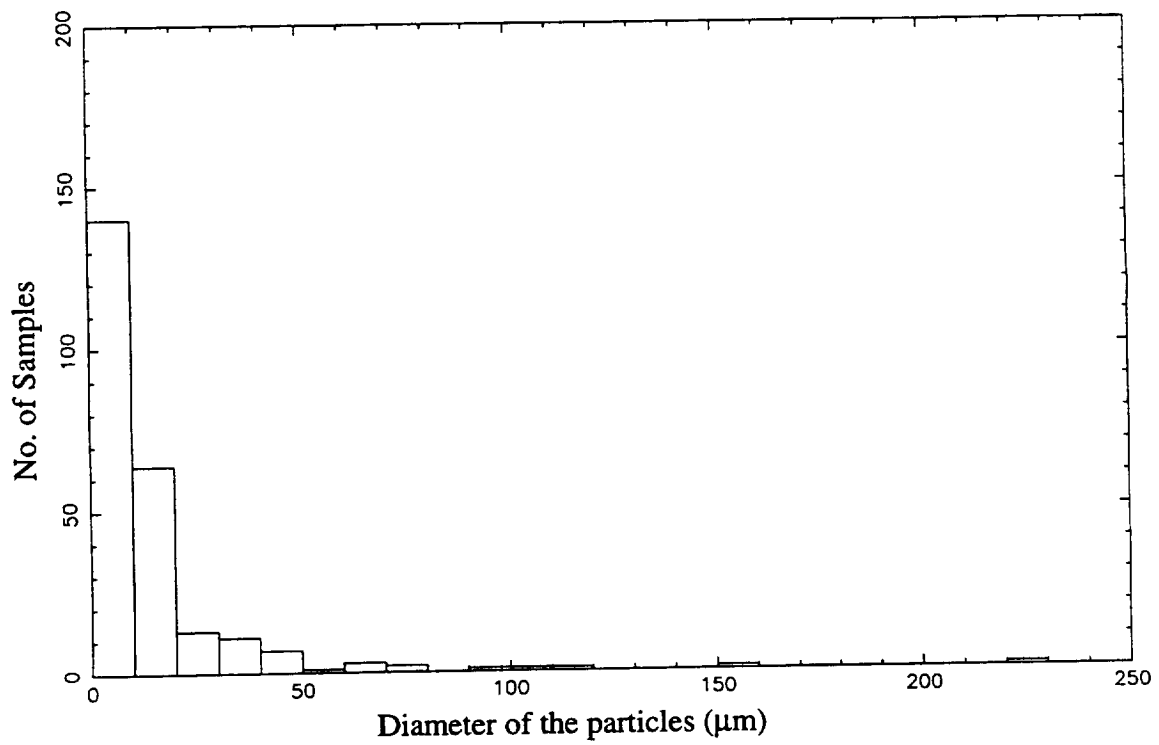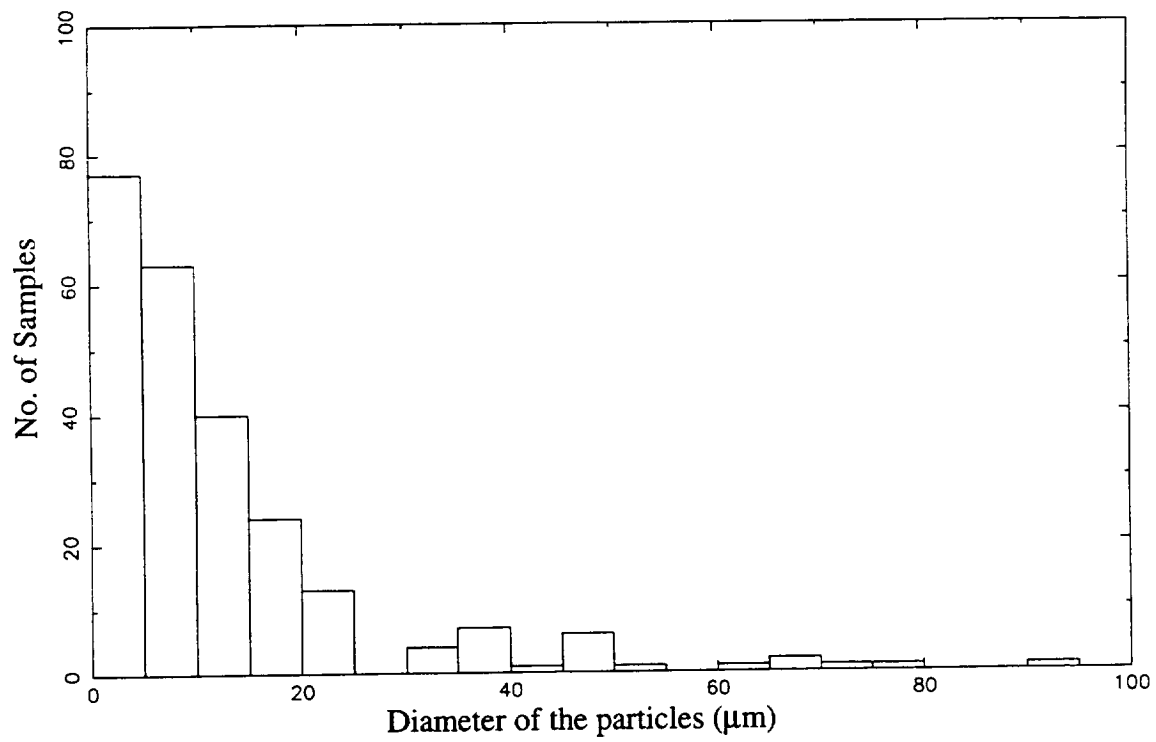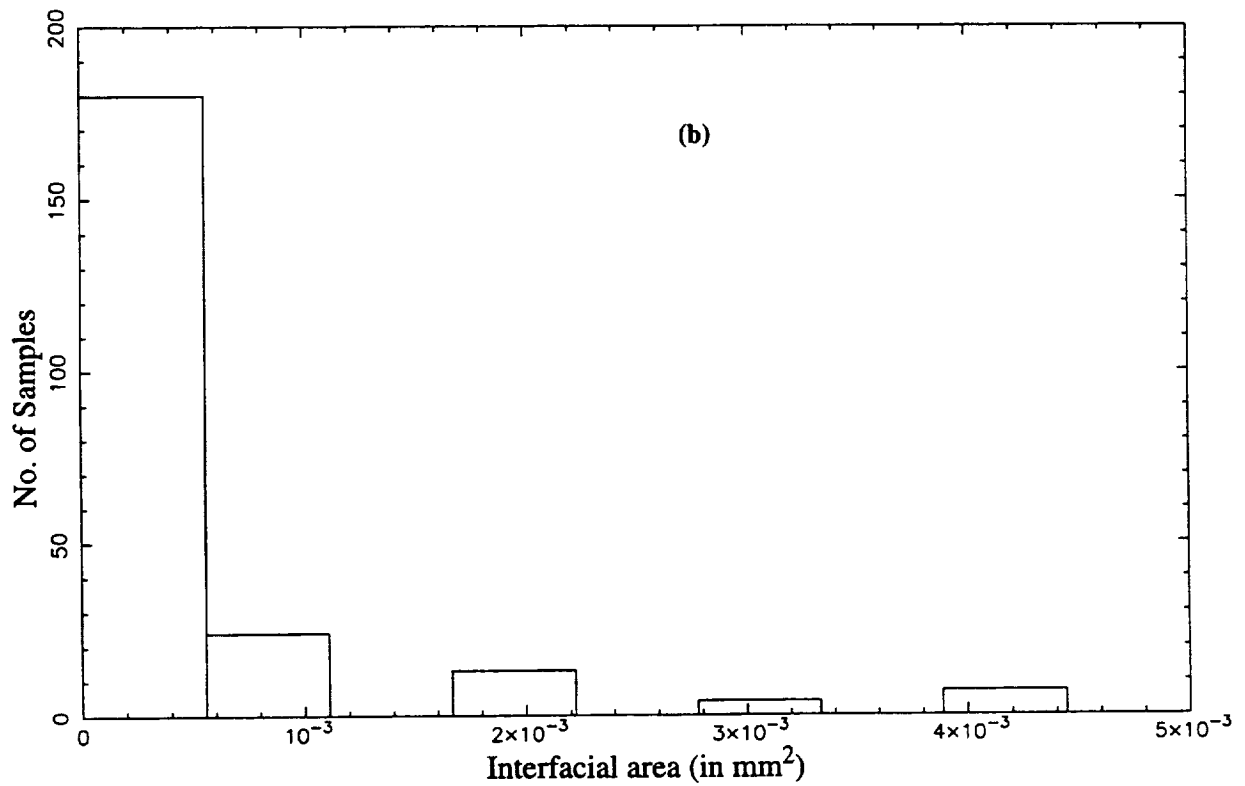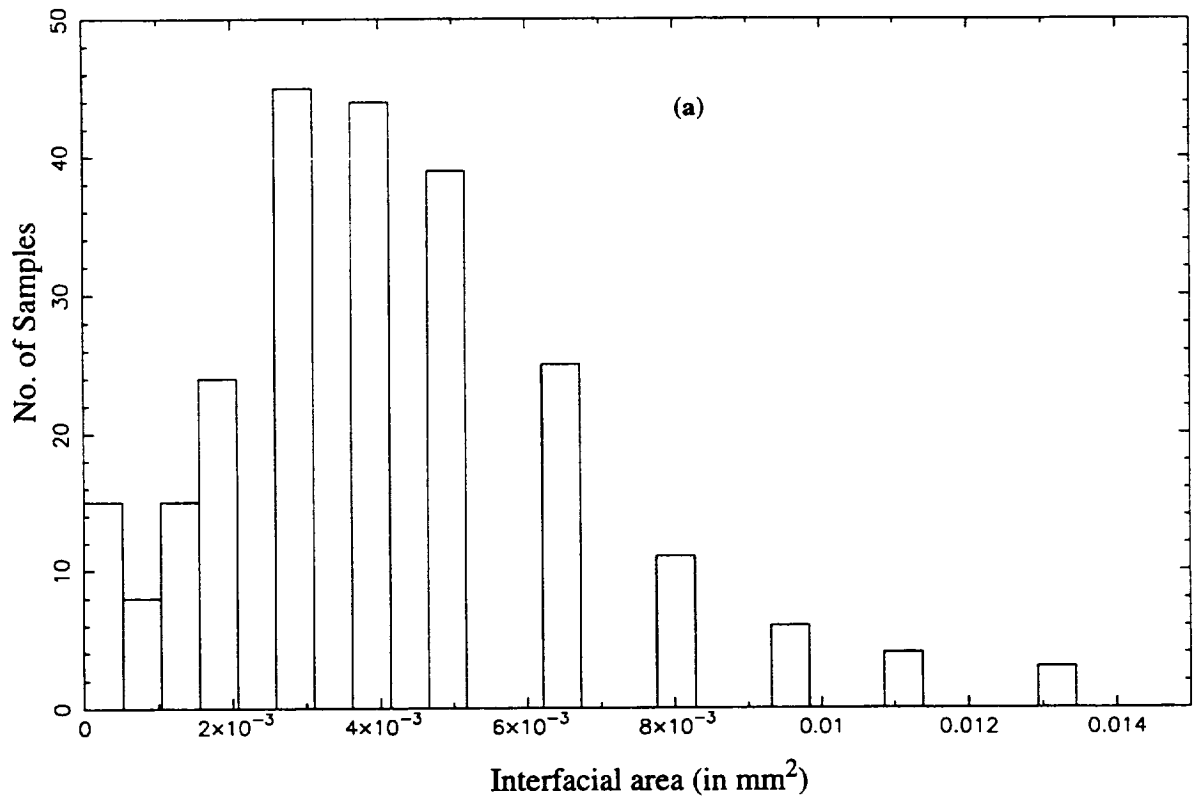
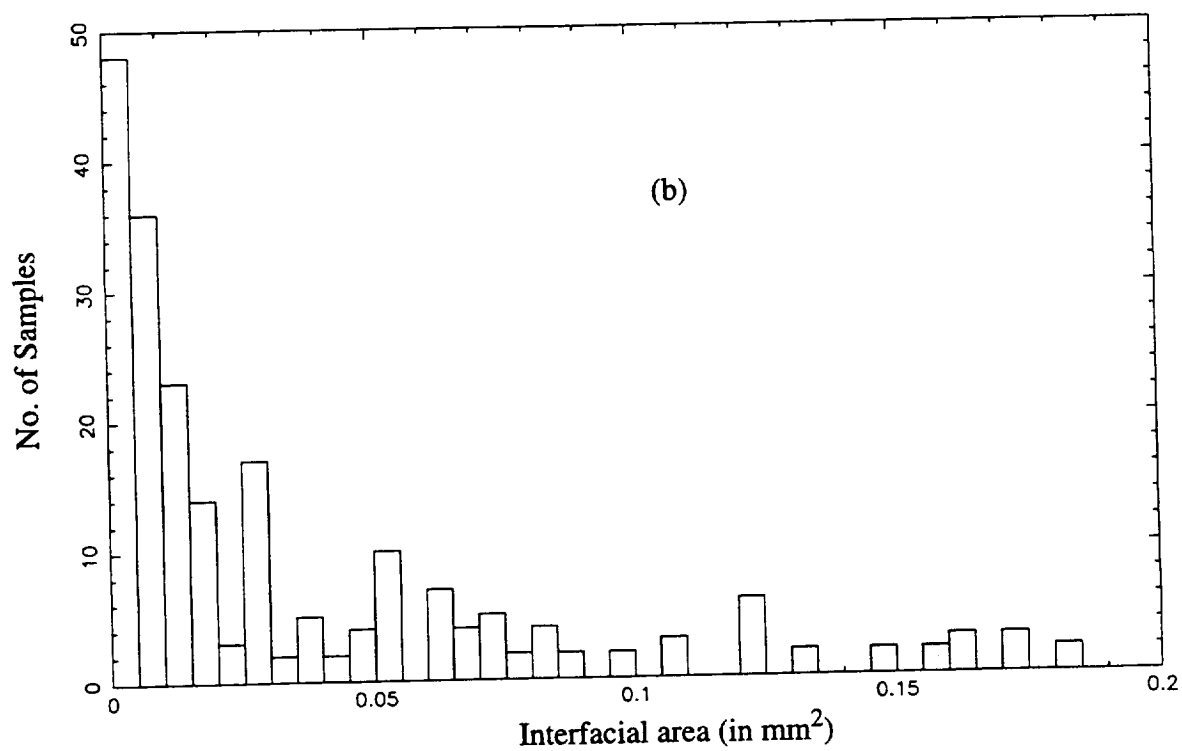**FIGURE 11. A typical distribution of particles (natural seeding) sizes in unseeded water**
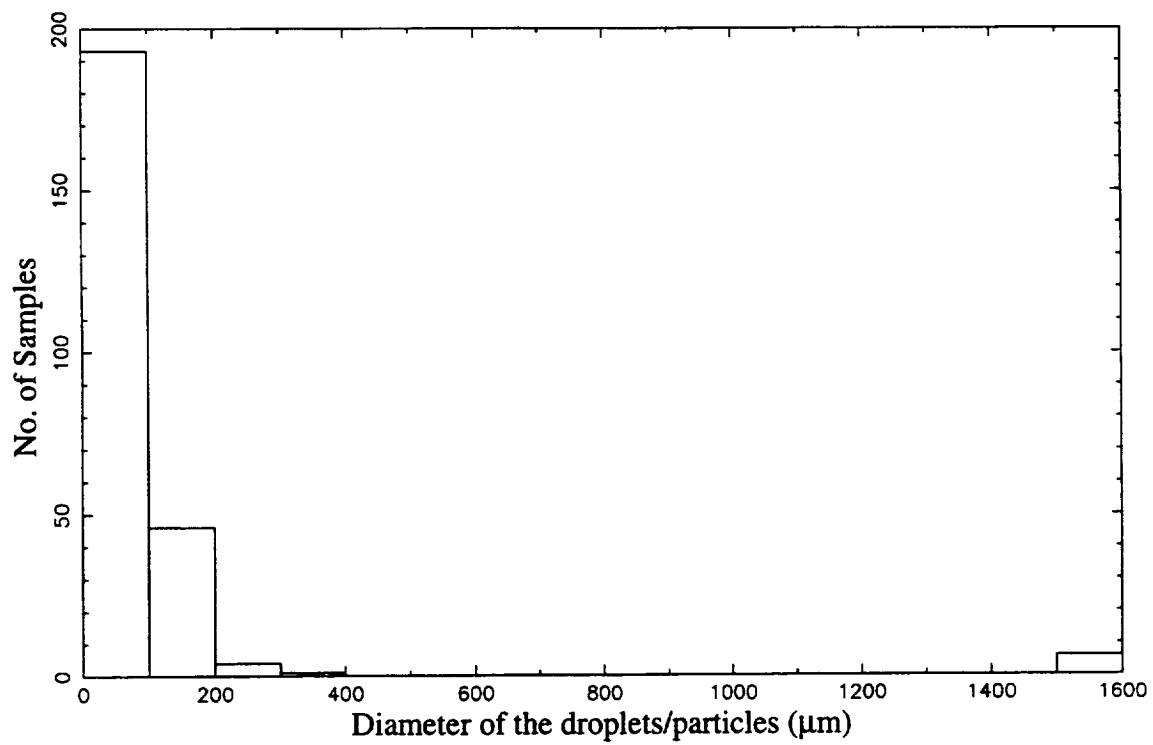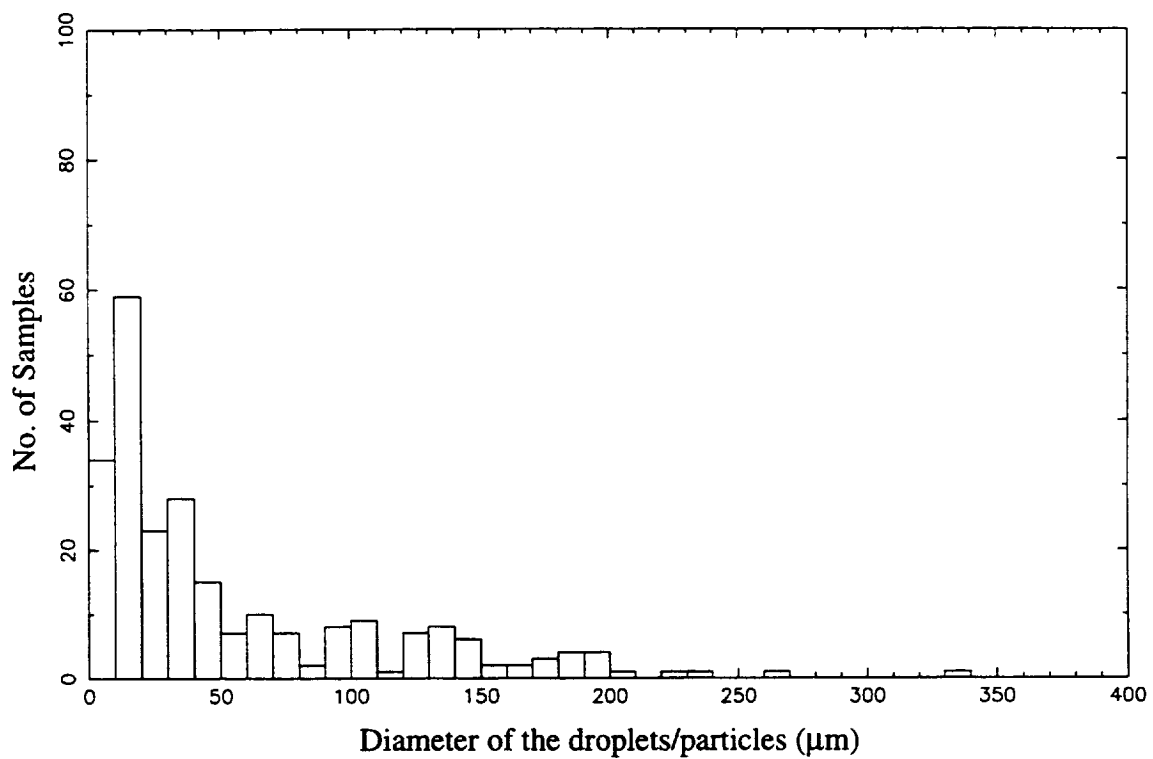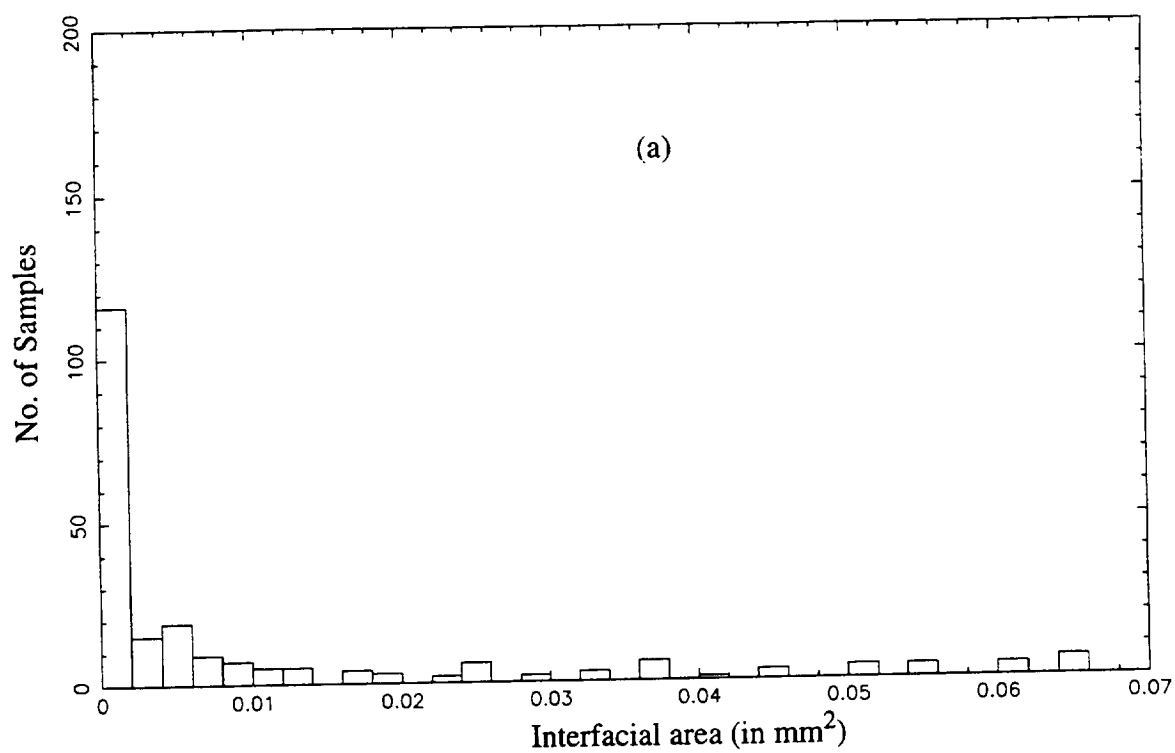
FIGURE 12. Typical oil droplet size distribution, Global void fraction=0.08%
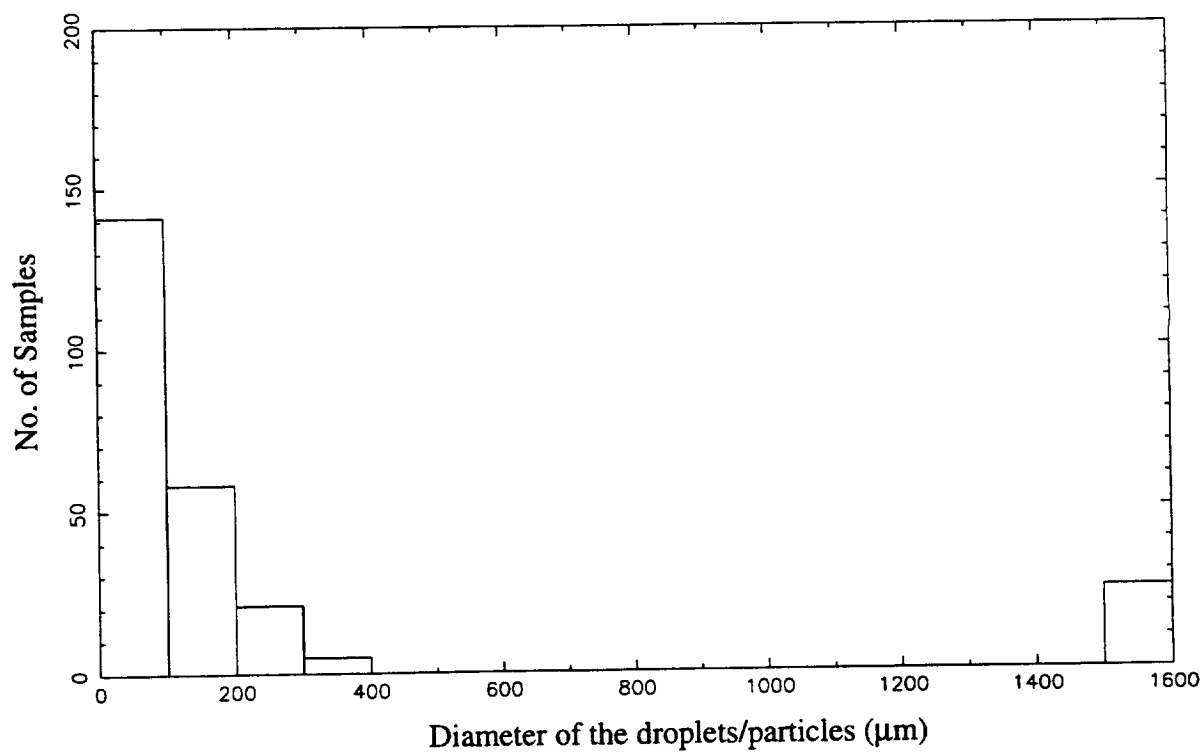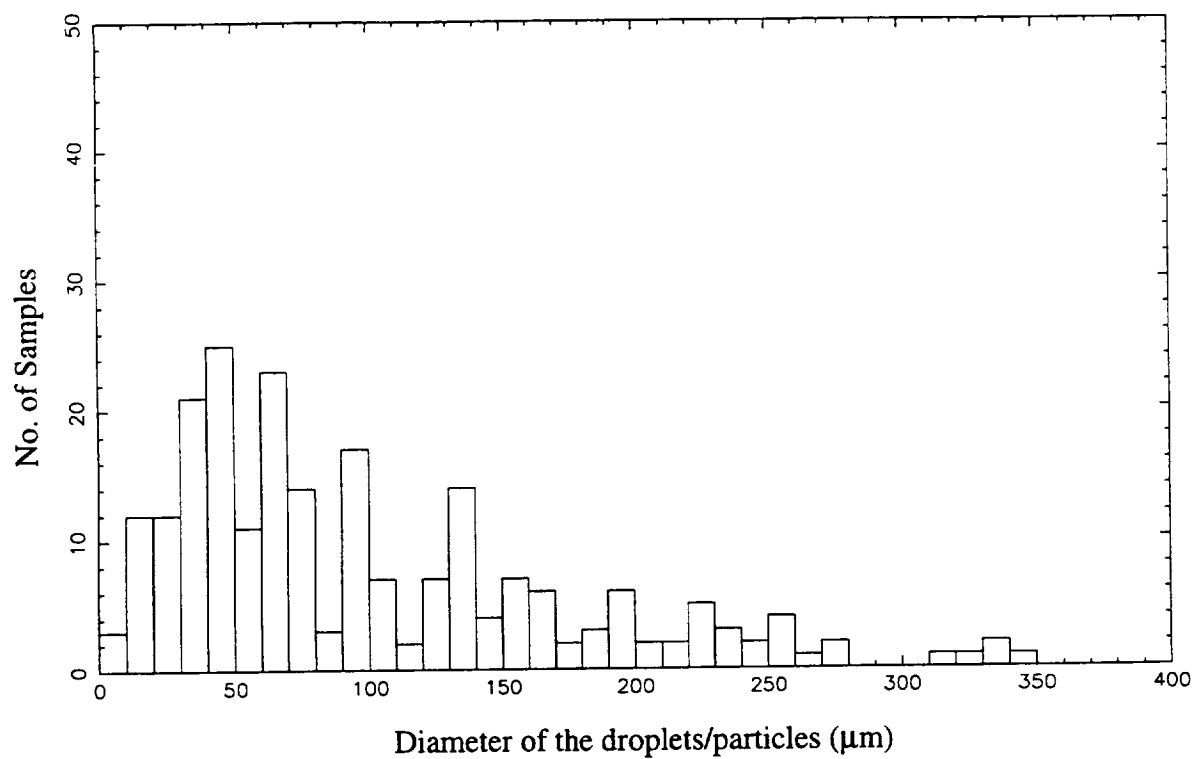
FIGURE 13. Typical oil droplet size distribution, Global void fraction=0.21%

FIGURE 14. Histogram for the interfacial area of particles: (a) with glass seeding (b) with natural seeding

FIGURE 15. Histogram of Interfacial area for (a) oil droplets corresponding to void fraction 0.07% (b)oil droplets corresponding to void fraction=0.2%

4.3 Work in Progress

With all the tests done outside the main loop, we are now ready to do the actual measurements of oil/water flows. The probes and necessary optics have been installed in the tank and the work is being done on the alignment of the probes. We are hoping that the larger oil droplets to be used will not form a film on the wall of the test section. Earlier experiments with the oil going through the pump showed such a tendency when the oil droplets were very small. However, with the new injector in the loop, it is unlikely that this will happen again. Needless to say the presence of the oil film on the wall is detrimental to our experiment.

4.4 Proposed future work

The main thrust of the future work is to put an experiment aboard the space shuttle. The objective of the experiment is to measure phase separation in an air/water mixture. The emphasis is on simplicity and efficiency in conducting the experiment and to provide adequate instrumentation of acquire a complete set of data. These data can then be used for further understanding the dynamics of bubbly flows in space. The instrumentation will consist of: (i) a two-dimensional pen Laser Doppler probe; (ii) a Phase Doppler Anemometer; (iii) a real time Fast Fourier Transform system, a phase discriminator, a high voltage generator and a demodulator, all fitted on a single PC card; (iv) a one-dimensional hot film anemometer; (v) a traversing mechanism, and (vi) a CCD camera. We will measure two-dimensional velocities with the LDA, one dimensional velocities and the local void fraction with the hot film probe, size distribution of the bubbles with the CCD camera and the FPDA. All these will be measured as a function of radial position for two axial locations: one close to the inlet and one close to the outlet. These data will allow us to compute bubble coalescence and breakup as well as the developing phase distribution. These instruments will be progressively tested and calibrated in experiments in drop-towers and parabolic

flights in Lear Jets. The loop itself will be a recirculating loop. A sine pump will circulate the mixture. For monodispersed experiments, we will separate the water from air using a centrifuge. For a arm length of 10 cm we will need about 600 rpm to simulate normal gravity. A specially designed injector will be used to generate the bubbles.

5.0 Bibliography

Alajbegovic, A., "*Phase Distribution and Turbulence Structure for Solid/Fluid Upflow in a Pipe*", Ph.D. Thesis, Rensselaer Polytechnic Institute, Troy, New York, 1994.

Arnold, G.S., "*Entropy and Objectivity as Constraints Upon Constitutive Equations for Two-Fluid Modeling of Multiphase Flow*", Ph.D. Thesis, Rensselaer Polytechnic Institute, Troy, New York, 1988.

Assad, A., "*An Experimental Study of Phase Distribution and Turbulence Structure for Solid/Liquid Flow in Horizontal and Vertical Pipes*", Ph.D. Thesis, Rensselaer Polytechnic Institute, Troy, New York, 1995.

Batchelor, G.K., "The Stress System in a Suspension of Force-Free Particles", J. Fluid Mechanics, Vol. 14, pp. 545-570, 1970.

Chapman, S. Cowling, T.G., "*The Mathematical Theory of Non-Uniform Gases*", Cambridge University Press, Cambridge, 1970.

Drew, D.A., Lahey, R.T., Jr., "The Virtual Mass and Lift Force on a Sphere in Rotating and Straining Inviscid Flow", Int. J. Multiphase Flow, vol. 13(1), pp. 113-121, 1987.

Drew, D.A., Lahey, R.T., Jr., "Some Supplemental Analysis on the Virtual Mass and Lift Force on a Sphere in Rotating and Straining Inviscid Flow", Int. J. Multiphase Flow, vol. 16(6), pp. 1127-1130, 1990.

Drew, D.A., Passman, S.L., "*Theory of Multicomponent Fluids*", To be published, 1995.

Hayworth, Curtis B, and Treybal, Robert E., "Drop Formation in Two-Liquid-Phase Systems", Industrial and Engineering Chemistry, Vol. 42, No. 6, June 1950.

Lahey, R.T., Jr., Drew, D.A., "The Current State-of-the-Art in the modelling of Vapor/Liquid Two-Phase Flows", ASME 90-WA/HT-13, 1990.

Nigmatulin, R.I., "Spatial Averaging in the Mechanics of Heterogenous and Dispersed Systems", Int. J. Multiphase Flow, vol. 5, pp. 353-385, 1979.

Null, Harold R., and Johnson, Homer F., "Drop Formation in Liquid-Liquid Systems from Single Nozzles", A.I.Ch.E. Journal, Vol. 4, No. 3, Sept. 1958.

Park, J-W., "*Void Wave Propagation in Two-Phase Flow*", Ph.D. Thesis, Rensselaer Polytechnic Institute, Troy, New York, 1992.

Serizawa A., Kataoka I., "Phase Distribution in Two-Phase Flow", *Transient Phenomena in Multiphase Flow*, Ed. Afghan, N,H., Hemisphere Pub. Corp., New York, pp. 179-225, 1988.

REPORT DOCUMENTATION PAGE

Public reporting burden for this collection of information is estimated to average 1 hour per response, including the time for reviewing instructions, searching existing data sources, gathering and maintaining the data needed, and completing and reviewing the collection of information. Send comments regarding this burden estimate or any other aspect of this collection of information, including suggestions for reducing this burden, to Washington Headquarters Services, Directorate for Information Operations and Reports, 1215 Jefferson Davis Highway, Suite 1204, Arlington, VA 22202-4302, and to the Office of Management and Budget, Paperwork Reduction Project (0704-0188), Washington, DC 20503.

1. AGENCY USE ONLY (Leave blank)	2. REPORT DATE	3. REPORT TYPE AND DATES COVERED
	March 1996	Final Contractor Report

4. TITLE AND SUBTITLE

Phase Distribution Phenomena for Simulated Microgravity Conditions: Experimental Work

5. FUNDING NUMBERS

WU–962–24–05
G–NAG3–1400

6. AUTHOR(S)

Maneesh Singhal, Fabian J. Bonetto, and R.T. Lahey, Jr.

7. PERFORMING ORGANIZATION NAME(S) AND ADDRESS(ES)

Rensselaer Polytechnic Institute
Center for Multiphase Flow
Troy, New York 12180

8. PERFORMING ORGANIZATION REPORT NUMBER

E–10138

9. SPONSORING/MONITORING AGENCY NAME(S) AND ADDRESS(ES)

National Aeronautics and Space Administration
Lewis Research Center
Cleveland, Ohio 44135–3191

10. SPONSORING/MONITORING AGENCY REPORT NUMBER

NASA CR–198461

11. SUPPLEMENTARY NOTES

Project Manager, John B. McQuillen, Space Experiments Division, NASA Lewis Research Center, organization code 6712, (216) 433–2876.

12a. DISTRIBUTION/AVAILABILITY STATEMENT

Unclassified - Unlimited
Subject Category 34

This publication is available from the NASA Center for Aerospace Information, (301) 621–0390.

12b. DISTRIBUTION CODE

13. ABSTRACT (Maximum 200 words)

This report summarizes the work accomplished at Rensselaer to study phase distribution phenomenon under simulated microgravity conditions. Our group at Rensselaer has been able to develop sophisticated analytical models to predict phase distribution in two-phase flows under variety of conditions. These models are based on physics and data obtained from carefully controlled experiments that are being conducted here. These experiments also serve to verify the models developed.

14. SUBJECT TERMS

Multiphase flow; Two phase flow; Reduced gravity; Voids; Bubbles

15. NUMBER OF PAGES

38

16. PRICE CODE

A03

17. SECURITY CLASSIFICATION OF REPORT	18. SECURITY CLASSIFICATION OF THIS PAGE	19. SECURITY CLASSIFICATION OF ABSTRACT	20. LIMITATION OF ABSTRACT
Unclassified	Unclassified	Unclassified	

NSN 7540-01-280-5500

National Aeronautics and
Space Administration

Lewis Research Center
21000 Brookpark Rd.
Cleveland, OH 44135-3191